Impact of polymeric stabilisers on the reaction kinetics of SrBr2

Solar Energy Materials & Solar Cells 238 (2022) 111648

Contents lists available at ScienceDirect

Solar Energy Materials and Solar Cells

journal homepage: www.elsevier.com/locate/solmat

Impact of polymeric stabilisers on the reaction kinetics of $SrBr_2$

Natalia Mazur [a,b], Sergio Salviati [c,d], Henk Huinink [a,b,*], Alberto Fina [c], Federico Carosio [c], Hartmut Fischer [e], Olaf Adan [a,b,e]

[a] Department of Applied Physics, Eindhoven University of Technology, Den Dolech 2, 5600, MB, Eindhoven, the Netherlands
[b] Eindhoven Institute for Renewable Energy Systems, Eindhoven University of Technology, PO Box 513, 5600, MB, Eindhoven, the Netherlands
[c] Dipartimento di Scienza Applicata e Tecnologia, Politecnico di Torino-Alessandria Campus, 15121, Alessandria, Italy
[d] Center for Sustainable Future Technologies, Istituto Italiano di Tecnologia, 10144, Torino, Italy
[e] TNO Materials Solutions, High Tech Campus 25, 5656, AE, Eindhoven, the Netherlands

ARTICLE INFO

Keywords:
Thermochemical energy storage
Salt hydration
Composite
Heat storage materials
Polyelectrolytes
Polymeric additives

ABSTRACT

Thermochemical heat storage (TCHS) in salt hydrates attracts increasing interest due to the high energy density combined with loss-free storage. Strontium bromide hexahydrate (SBH), and composites thereof, are often suggested as suitable materials for this application. Although many aspects of SBH composites have been thoroughly investigated, very little has been done on the fundamental aspects of the hydration reaction and interactions between composite components on a molecular level. In this paper, we examine the interaction between SBH and polymeric additives polydiallyldimethylammonium chloride (PDAC), sodium carboxymethyl cellulose (CMC), and polyacrylic acid (PAA) in previously developed TCHS composites. The primary function of the polymeric additives is enhanced mechanical integrity however this study investigates potential implications on reaction temperature and speed the addition of such components might have. Focus is given to the interaction between $SrBr_2$ and PDAC since such composites showed (de)hydration behaviour deviating from pure $SrBr_2$. The reaction kinetics are investigated at several points in the phase diagram through thermogravimetric analysis (TGA), supplemented by powder x-ray diffraction (XRD) studies. Our findings show that there exists an interaction between $SrBr_2$ and PDAC which manifests itself through shrinkage of crystallite size and increased lattice strain induced by preferential binding of PDAC to $SrBr_2$. Depending on the PDAC content in the composite we have found out that 1) at excessive amounts PDAC inhibits hydration due to its sequestering properties 2) at low amounts it an enhances reaction kinetics due its hydrophilic nature.

1. Introduction

Energy storage technologies comprise various techniques to store electrical and thermal energy and are considered a key field for developing smart energy systems to mitigate climate change [1]. In addition, innovative thermal storage technologies (TES) can reduce CO_2 emissions, together with system efficiencies improvements and lower costs [2].

Thermochemical heat storage (TCHS) is one of the main types of TES. In this system, a solid/gas reversible reaction is used to store the energy. While different sorption mechanisms and solid/gas working pairs were evaluated [3], hydration/dehydration reactions between salt hydrates and water vapour are widely studied for TCHS applications. The reason for that is their high energy storage densities [4], reaction temperatures suitable for low-grade heat storage, competitive costs and low health and safety risks [5]. These properties motivated the development of prototypal TCHS systems in different fields, such as buildings heating [6], solar heat storage [7], power-to-heat solutions [8] and industrial heat recovery [9]. However, while TES is considered a promising technology in all these applications, it is evidenced that further advances in terms of both material and system design are required to obtain valuable solutions [10].

The TCHS system based on salt hydrates is charged by delivering heat to the hydrated material, resulting in desorption of water, which is then isolated from the salt during storage. This guarantees a long-term loss-free energy storage capability, which is a great advantage over other TCHS methods. When heat is needed, water vapour and the solid phase are brought together to trigger the sorption reaction, which discharges the system [11].

One of the major drawbacks of using salt hydrates is their integrity

* Corresponding author. Department of Applied Physics, Eindhoven University of Technology, Den Dolech 2, 5600 MB, Eindhoven, the Netherlands.
E-mail address: h.p.huinink@tue.nl (H. Huinink).

https://doi.org/10.1016/j.solmat.2022.111648
Received 3 August 2021; Received in revised form 20 January 2022; Accepted 6 February 2022
Available online 16 February 2022

during cycling [12] and the possibility of deliquescence occurring during operation [13]. Further disadvantages of salts are enhanced metal corrosion [14], as well as low thermal conductivity (0.7–1.0 W/mK) that affects the heat transfer between TES and the environment [15].

A wide variety of salt hydrates was investigated in literature for TCHS purposes and classified using properties such as hydration/dehydration temperatures and energy storage densities [16]. In this work, Strontium Bromide Hexahydrate (SBH) was chosen as TCHS material because it presents high cyclic stability [17], a high energy storage density of 798 J/g (1.95 GJ/m^3 or 542 kWh/m^3), operating temperatures below 100 °C [18] and it was also effectively applied in preliminary thermochemical reactors [19–22]. In particular, the reversible reaction between strontium bromide hexahydrate and strontium bromide monohydrate (SBM), shown in reaction, is under consideration in this study:

$$SrBr_2{\cdot}6H_2O(s) \leftrightarrow SrBr_2{\cdot}H_2O(s) + 5H_2O(g)$$

Similarly to other salts hydrates used for TCHS, SBH suffers from drawbacks concerning cyclic grain stability and thermal conductivity. An established approach to overcome those limitations is the preparation of composites in which the salt is incorporated into a porous matrix [22]. Expanded Graphite (G) was investigated as a matrix by Zhao et al. [23]. It is highly porous and conductive support for SBH, which enhances thermal conductivity and permeability. Cammarata et al. [24] studied similar composites and revealed enhanced kinetics and a reduced hysteresis between reaction temperatures with the addition of the matrix. To enhance the mechanical stability of SBH-G composites, Salviati et al. [25,26] added hydrophilic polymers like polydiallyldimethylammonium chloride (PDAC) and carboxymethyl cellulose (CMC) to the material and proved greater cyclability on a tablet level. In addition to graphitic materials, other matrixes, such as metal-organic frameworks [27] and silica gel [28], have been studied. Most recently, Ding et al. [29] have developed an SBH-expanded vermiculite composite with high energy density. Additionally, they have investigated the kinetic properties of (de)sorption reactions with the aid of classical solid-state reaction models. While these works demonstrate the increased mechanical stability and thermal conductivity of SBH-composite materials, the need for a deeper understanding of the physical chemistry phenomena, such as (de)hydration mechanisms, concerning the thermochemical process must be addressed.

Sögütoglu et al. [30,31] studied the hydration/dehydration mechanism of pure salt hydrates. Their studies showed that many salts have a so-called metastable zone (MSZ) in which kinetics are strongly hindered as nucleation of the newly to-be-formed phase is problematic. This effect causes a shift in the operational hydration/dehydration temperatures away from the equilibrium conditions, thus defining the Metastable Zone Width (MZW). Furthermore, the studies indicated that the hydration reaction proceeds through water adsorption, forming a wetting layer on the surface of the lower hydrate [32]. It then leads to the dissolution of ions from the lower hydrate, followed by recrystallisation of the higher hydrate within that wetting layer. Ion mobility within the wetting layer is crucial as it facilitates the reaction and determines MZW. Studies on $MgSO_4$ and Na_2SO_4 [33] have also indicated that liquid intermediate states could play a vital role in the hydration process, where otherwise a slow solid-solid phase transition would occur.

Thy hydration mechanism proposed by Sögütoglu et al. is analogous to salt crystallisation from solution. It is well known that polymers might impact nucleation, crystal growth or crystal habit when a polymeric additive is present in the stock solution [34,35]. Earlier studies have shown that PDAC can impact the shape and size of $CaCO_3$ crystals [36]. However, when added to CaF_2 supersaturated solution, PDAC had almost no impact on the crystal growth rate, which was strongly affected by even small amounts of polyacrylic acid (PAA) [37]. On the contrary, PDAC has been found to be a strong crystallisation inhibitor in a calcium-arsenic-hydroxyapatite system due to electrostatic interactions on the molecular surface [38]. Nevertheless, no studies have been found that investigate the impact of polymers or polyelectrolytes on salt hydrates' (de)hydration behaviour on a fundamental level.

This study aims to understand the impact polymeric additives in TCHS composites can have on the hydration/dehydration transition of the salt hydrate. Three polymers (anionic CMC and PAA and cationic PDAC), which in earlier work have been shown to stabilise SBH-G composites [25,26] mechanically, are investigated with thermogravimetric analysis, powder x-ray diffraction, and dynamic vapour sorption. The focus is given to PDAC-SBH interaction and its implications on the phase transitions of the salt hydrate.

2. Materials and methods

2.1. Materials

$SrBr_2{\cdot}6H_2O$ with >95% purity in powder form was purchased from Alfa Aesar. Expanded natural graphite (G) was purchased from TIMCAL, commercial-grade TIMREX® BNB90 with a bulk density of 0.03 g/cm^3, a surface area of 28.4 m^2/g and an average particle size of 85 μm, as reported in the material datasheet. Polydiallyldimethylammonium chloride (PDAC) with a molecular weight of 400,000–500,000 g/mol was purchased from Merck as a 20% wt/wt water solution. Sodium carboxymethyl cellulose (CMC) with an average molecular weight of 250,000 g/mol and a degree of substitution of 0.7 was purchased from Merck. Polyacrylic acid (PAA) was purchased from Merck as a 35% wt/wt water solution and presented an average molecular weight of 100,000 g/mol as declared by the producer. Sodium Hydroxide (NaOH) pellets with 99.8% purity were purchased from Merck. $SrCl_2{\cdot}6H_2O$, technical grade in powder form, was purchased from Alfa Aesar. All reagents were used as received for preparing stable water dispersions using deionised water supplied by a Direct-Q® 3 UV Millipore System (Milano, Italy).

2.2. Samples preparation

The composite materials were prepared using a wet impregnation technique adapted from Ref. [25]. At first, the graphitic materials (3 g) were dispersed in water (90 ml) in a beaker, using magnetic stirring. After that, 1.5 g of the selected binder was added to the beaker in the form of a water solution/dispersion. PDAC was added as received in the form of water-based solutions, while CMC was first dissolved in water with magnetic stirring for 1 h before adding it to the graphite dispersion. PAANa (polyacrylic acid sodium salt) was prepared from a stoichiometric mixture of NaOH and PAA dissolved in water and subsequently added to the graphite dispersion. Finally, SBH was added to the dispersion, and it was stirred overnight. Water was then evaporated over a heated plate at 100 °C under continuous magnetic stirring.

The weight ratios of the materials components and the molar ratios of monomers to pure $SrBr_2$ are listed in Table 1.

Table 1
List of the prepared composite materials. The reported values are dry weight ratios between the sample's components.

Sample	SBH [g]	G [g]	Polymer [g]	Polymer type	mol monomer : mol $SrBr_2$
SBH	1	0	0	None	0
SBH_G	5	1	0	None	0
SBH_G_PAANa	5	1	0.5	PAANa	0.379
SBH_G_CMCNa	5	1	0.5	CMCNa	0.136
SBH_G_PDAC (0.1)	5	1	0.1	PDAC	0.044
SBH_G_PDAC (0.5)	5	1	0.5	PDAC	0.221
SBH_G_PDAC(1)	5	1	1	PDAC	0.442
SCH_G_PDAC(1)	3.75[a]	1	1	PDAC	0.442[a]

[a] Here, the weight and molar ratios refer to $SrCl_2{\cdot}6H_2O$ instead of $SrBr_2{\cdot}6H_2O$ content used in the synthesis.

Sample SBH was used as a reference and characterised as received in powder form. SBH_G, used as a reference, was prepared with the same procedure used for the other composite materials, omitting the polymer addition step.

2.3. Characterisation

2.3.1. Pressure-temperature (p-T) measurement

The equilibrium line between $SrBr_2$ hexahydrate and monohydrate was measured using an in-house developed setup illustrated in Fig. 1. The setup is built from 6 mm stainless steel tubing and Swagelok connections and valve. The sample chamber is connected with a KF flange fitted with an o-ring and a circumferential clamp. It is heated with an electrical heating mantle whose temperature is controlled with a Eurotherm controller. The temperature and pressure data are collected through an Arduino connected to a computer. The temperature of the thermocouple is calibrated against a well-defined temperature source, and it is within ±0.1 °C range. The pressure sensor used in the setup has an accuracy of 0.2%.

Approximately 3g of as received SBH was loaded into the sample chamber. The setup was then evacuated, and changes in its pressure as a function of temperature were measured continuously. The sample was heated up in steps of 10 °C from 20 °C to 80 °C with a dwell time of 2 h per step. By fitting the acquired data points with van 't Hoff equation, Equation (1), a line describing the p-T relationship between hexahydrate and monohydrate can be constructed.

$$p_{eq} = p_0 e^{\frac{\Delta H^0}{RT} - \frac{\Delta S^0}{R}} \quad (1)$$

where p_{eq} [mbar] is the measured vapour pressure, p_0 is the reference pressure of 1013 mbar, ΔH^0 [$JK^{-1}mol^{-1}$] is the standard molar reaction enthalpy, ΔS^0 [$Jmol^{-1}$] is the standard molar entropy, R is the standard gas constant (8.3145 $JK^{-1}mol^{-1}$), and T [K] is the applied temperature corresponding to the measured vapour pressure.

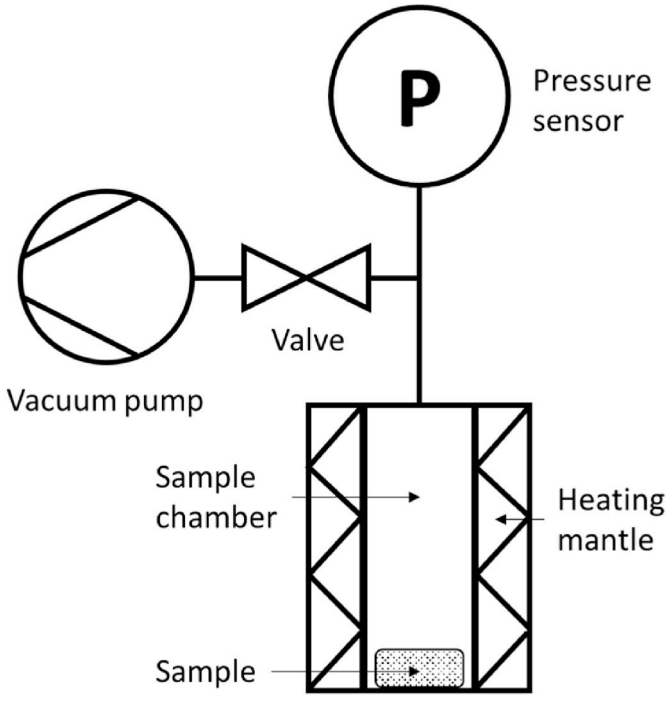

Fig. 1. A schematic representation of the p-T setup. Except for the external vacuum pump, the entire system is thermally insulated. The sample chamber is heated with an electrical heating mantle, and the absolute pressure in the system is measured with a pressure sensor.

2.3.2. Thermogravimetric analysis

Reaction kinetics were studied in a thermogravimetric analyser (TGA) by Mettler-Toledo TGA/DSC3+ LF1100. The temperature of TGA was calibrated using a heat flow signal of melting points of naphthalene, indium and zinc, giving an accuracy of 0.2 °C. An external humidifier was coupled with the TGA, and it was calibrated by establishing deliquescence point of $LiCl{\cdot}H_2O$, $K_2CO_3{\cdot}1.5H_2O$, $MgCl_2{\cdot}6H_2O$ and $Mg(NO_3)_2{\cdot}6H_2O$ salt hydrates at 25 °C [39] with an accuracy of 0.16 mbar. All experiments were conducted under a nitrogen atmosphere with a fixed flow rate of 300 mL/min.

Before all TGA measurements, samples were prepared by drying in an oven at 50 °C to drive the water out of the polymeric additives. It makes it possible to grind the samples in a pestle and mortar and subsequently sieve between 50 and 164 μm fractions. Approximately 5 mg of prepared sample was loaded into a 40 μL Mettler-Toledo standard aluminium pan without a lid.

(De)hydration onset points were measured at several fixed water vapour pressures (4, 6, 8, 12 and 15 mbar, green arrows in Fig. 2) by scanning through a temperature range between 25 and 60 °C at a rate of 0.1 °C/min. After each temperature scan, the temperature was held constant for 3 h to ensure complete conversion before proceeding to the following temperature scan. Reaction onset points were determined from 1st derivative plots as illustrated in Fig. 3. The 1st derivative of the mass-time curve was calculated and plotted against the measured sample temperature. The temperature corresponding to an abrupt change in the 1st derivative is taken as the reaction onset point. It is defined as a cross point between a horizontal line drawn where the 1st derivative equals zero and a tangent is drawn at the point corresponding to the fastest change in mass.

Before measuring reaction kinetics, samples were subjected to 10 (de)hydration cycles to minimise the impact of morphology or the sample's thermal history on the measurement [30,40]. Hydration was conducted at isothermal and isobaric conditions, 30 °C and 12 mbar, while dehydration occurred at 85 °C and 0 mbar. Reaction kinetics were measured at a sample temperature of 45 °C and four different water

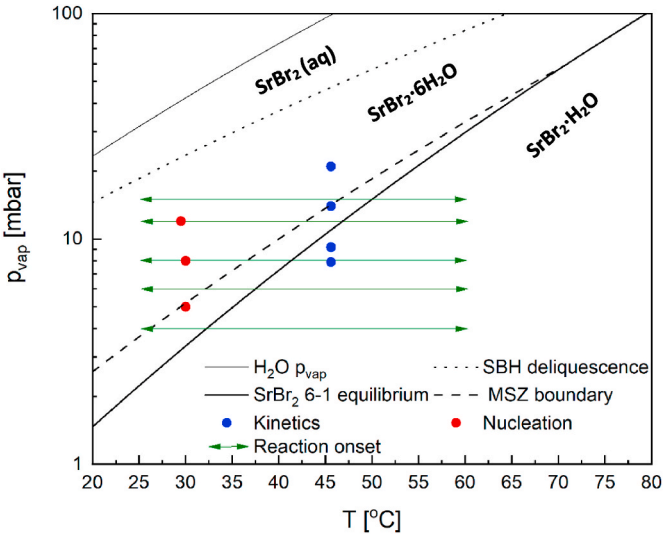

Fig. 2. Pressure-Temperature phase diagram of $SrBr_2$ indicating measurement conditions. The thick solid black line is the equilibrium line between SBM and SBH; the dashed line indicates the MSZ boundary of SBM hydration, dotted shows deliquescence of SBH, while the thin black line shows the saturation vapour pressure of pure water. Green arrows indicate conditions of isobaric measurements determining reaction onset points; red dots show conditions at which nucleation and growth study was conducted, and blue dots show conditions at which isobaric and isothermal reaction kinetics were investigated. (For interpretation of the references to colour in this figure legend, the reader is referred to the Web version of this article.)

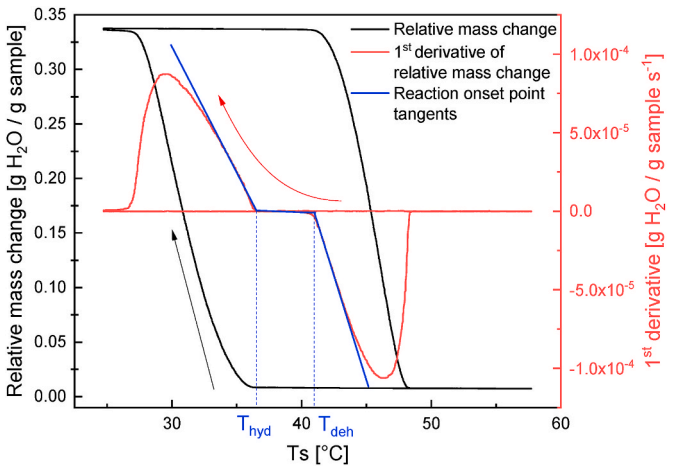

Fig. 3. An example of the method used to determine the reaction onset points. The black plot shows the relative mass change of pure $SrBr_2$ at 8 mbar as a function of measured sample temperature. The red plot is the 1st derivative of the black plot. The blue solid lines show the tangents drawn to determine the reaction onset points while the arrows indicate reaction direction. (For interpretation of the references to colour in this figure legend, the reader is referred to the Web version of this article.)

vapour pressures (p_{vap}), 21 and 14 mbar in case of hydration and 9 and 8 mbar for dehydration (blue dots in Fig. 2). Preceding the isobaric and isothermal hydration, the sample was dehydrated to monohydrate at 85 °C and 0 mbar, after which temperature was lowered to 45 °C and allowed to equilibrate for 30 min while maintaining 0 mbar before vapour pressure was increased to the desired value and maintained constant for at least 1.5 h. To investigate the dehydration kinetics, the sample was first hydrated at 45 °C and 21 mbar before the vapour pressure was lowered to the desired value and kept constant for 2 h.

2.3.3. Powder X-ray analysis

Powder X-ray analysis (XRD) was conducted in Rigaku MiniFlex 600 X-ray diffractometer equipped with Cu Kα X-ray source, a Be monochromator (λ = 1.5419 Å, 40 kV, 15 mA), a D/tex Ultra2 1D detector and an Anton-Paar BTS500 heating stage. All measurements were done between 10 and 80 2θ with 0.02° step size and a scan speed of 5°/min. All samples were ground and dried in an oven at 60 °C for over 24 h before powder patterns of SBM with or without additives were measured. Dry air flow was supplied during the measurement to avoid any hydration. Subsequently, samples were hydrated in a desiccator over a saturated $MgCl_2$•$6H_2O$ solution (33%RH; ≈8 mbar at 21 °C) for over 48 h before powder patterns of SBH with and without additives were recorded. A saturated $MgCl_2$•$6H_2O$ solution was chosen as a fixed source of water vapour due to its desirable partial pressure, which allows fast reaction kinetics without risk of deliquescence. Rigaku PDXL2 software was used to analyse the data. Measured patterns were matched against patterns found in Crystallography Open Database (COD) [41].

2.3.4. Dynamic vapour sorption

The sorption properties of pure PDAC were investigated employing the dynamic vapour sorption (DVS) thermogravimetric method with Q5000 SA thermobalance from TA Instruments. Due to the presence of a reference pan, this method allows for exact and long-term measurements of (de)sorption isotherms. PDAC powder was prepared by drying as received solution in an oven at 100 °C to evaporate all the solvent. The solid polymer was then pulverised in a pestle and mortar, and approximately 1 mg of powder was used for the measurement. A quartz crucible was used for DVS measurement, which always started with a 1 h in-situ drying step at 80 °C and 0 mbar. Subsequently, the chamber's temperature was lowered to the desired value (25, 35 and 40 °C), and mass was equilibrated at dry conditions. Then relative humidity (RH) was stepped from 0 to 60% in steps of 5% with a dwell time of 5 h per step. The measurements were conducted under a nitrogen atmosphere with a fixed flow rate of 200 mL/min. The temperature is measured with an accuracy of 0.1 °C, while the vapour pressure is calibrated with the known deliquescence points of several salt hydrates [39] and supplied with an accuracy of 1% RH.

2.4. Single crystal growth

The impact of amine groups on the crystallisation behaviour of $SrBr_2$·$6H_2O$ was investigated through single crystal growth from solution. For this study, $SrBr_2$·$6H_2O$, purchased from Alfa Aesar, N-Methyl-2-Pyrrolidone (NMP) purchased from Biosolve, and 20% wt/wt high molecular weight PDAC water solution, purchased from Aldrich, were used. 2 g of SBH was dissolved in 2 mL of deionised water in a glass vial. To that, either NPM or PDAC solution was added in the same ratio as used for SBH_G_PDAC(1) composite. Additionally, a solution mimicking SBH_G_PDAC(0.1) composite and a reference with pure SBH were prepared. The solutions were further diluted with water till the total content of added water was equal to 4 mL. Vials were covered with perforated parafilm and placed in a desiccator with silica gel until crystals appeared in the solution (90–100 days). Crystals were removed from the solution, and the excess mother liquor was dabbed off with tissue paper before they were photographed. A previously conducted SEM study on SBH_G_PDAC composites [25] can be consulted for a more detailed picture of the micromorphology of the complete composite.

3. Results

3.1. Phase diagram and metastability

3.1.1. Pure $SrBr_2$

To assess the effect of additives on phase transitions of $SrBr_2$, we first need to characterise the (de)hydration behaviour of the pure salt hydrate. A p-T phase diagram in Fig. 4 maps out the reaction conditions for pure $SrBr_2$ hexa-monohydrate transitions. We have obtained the

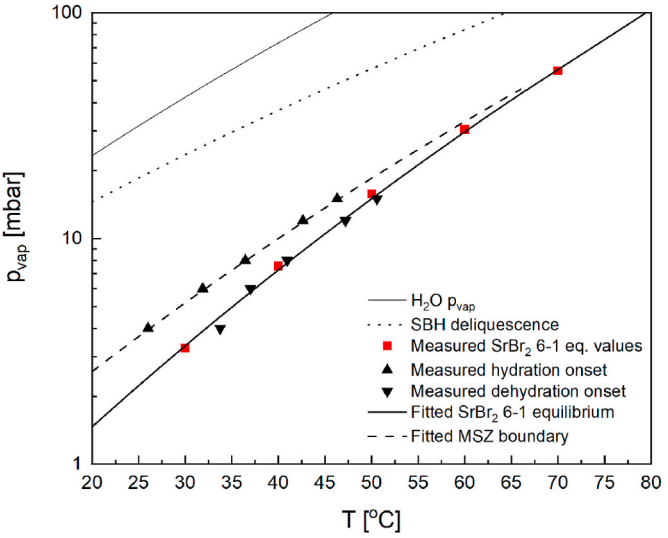

Fig. 4. p-T phase diagram of pure $SrBr_2$ showing saturation vapour pressure of pure water (blue line), deliquescence vapour pressure of SBH [42] (dotted line), measured equilibrium conditions between SBH and SBM (red squares) and the fit based on Eq. (1) (thick solid line) Measured reaction onset points are indicated with triangles, with upwards triangles being hydration of SBM, and downwards triangles being dehydration of SBH. The dashed line is a fit of hydration onset based on Eq (1), and it indicates the edge of MSZ. (For interpretation of the references to colour in this figure legend, the reader is referred to the Web version of this article.)

equilibrium line by measuring equilibrium vapour pressure at set temperature using an in-house developed p-T measurement setup. Van 't Hoff fit of measured values (red squares) results in a reaction enthalpy and entropy of 61 kJ/mol and 154 J/K mol, coinciding with literature values [16,20]. Inserting the thermodynamic values into Equation (1) over a range of temperatures gives the fitted equilibrium line (solid black line).

With the equilibrium line for 6-1 transition well-defined reaction, we can now determine reaction onset points at specific vapour pressures. Those were measured at isobaric conditions (4, 6, 8, 12, 15 mbar) by scanning through a temperature range (25–60 °C 0.1 °C/min). Black triangles in Fig. 4 indicate measured reaction onset points. The plot hardly shows metastability in the case of dehydration, while a significant metastable zone is present for hydration (dashed black line). Esaki et al. [44] investigated 6-1 transition and found a negligible deviation from the hydration and dehydration reaction equilibrium conditions, which contradicts our present findings. Deviation in the onset of both hydration and dehydration reaction is known for many other salt hydrates [17,30]. On the other hand, the absence of metastability for dehydration is striking. To the best of the authors' knowledge, such asymmetric reaction behaviour was not observed in the past.

3.1.2. The influence of polymers

With the phase transition behaviour of pure $SrBr_2$ mapped out in a phase diagram, Fig. 4, we can assess the impact of other composite components. Initial screening of 4 composites, 3 of which had identical polymer content (0.5 g polymer: 1 g G: 5 g SBH) and one that comprised only SBH and graphite (5 g SBH: 1 g G), was conducted in two steps. First, we performed a series of TGA measurements, followed by phase characterisation in XRD.

The TGA screening was conducted at isobaric conditions (p_{vap} =12 mbar, T= 25–60 °C), and the data is plotted in Fig. 5. The grey lines relate to pure $SrBr_2$, used for reference, while the coloured lines belong to investigated composite materials. In all cases, the relative water absorption by a composite is lower than for pure $SrBr_2$ primarily due to graphite, which has no water sorption ability. From this data, we can conclude that presence of graphite in the composite (black) has a marginal effect on the reaction onset points. We can draw a similar conclusion for composites with CMCNa (green) and PAANa (orange), which both have little to no impact on the measured (de)hydration onset points. Interestingly, the hydration behaviour is strongly influenced by the presence of PDAC (blue). The significant lowering of hydration temperature by 2.5 °C indicates an interaction between the salt and the polymer.

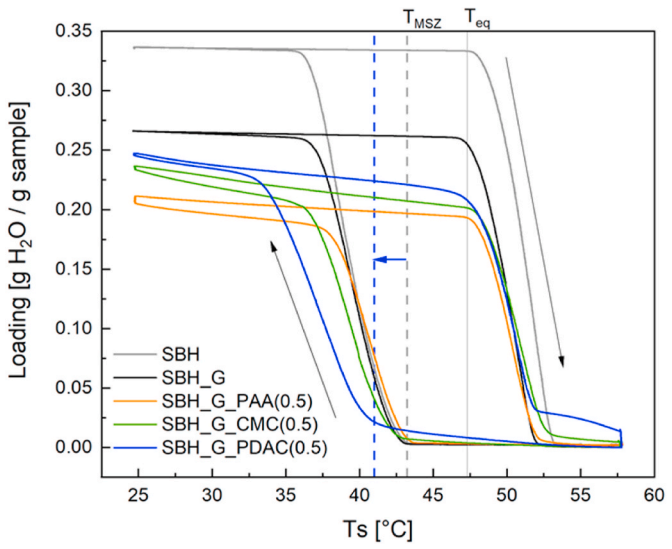

Fig. 5. Relative mass change vs measured sample temperature measured at a fixed vapour pressure of 12 mbar for pure SBH (grey), SBH_G (black) and SBH_G_polymer composites (PAA-orange, CMC-green, PDAC-blue). Black arrows indicate the direction of the mass change. Grey lines indicate reaction onset points of pure SBH, with T_{eq} being the measured equilibrium line and T_{MSZ} being the measured MSZ boundary. The coloured dashed line indicates a shift in hydration of SBH_G_PDAC(0.5). (For interpretation of the references to colour in this figure legend, the reader is referred to the Web version of this article.)

For the second part of the screening in XRD, the desired phase was prepared ex-situ through sample dehydration in an oven at 60 °C to obtain SBM or hydration in a desiccator with a fixed relative humidity of 33% to obtain SBH. Previous studies [25,26] have shown that the crystalline structure of $SrBr_2$ is preserved in the presence of graphite and PDAC, and we expect the same for composites with CMCNa and PAANa, given we have not seen any significant changes in (de)hydration behaviour in the first part of the screening.

In Fig. 6, we can see that both SBM and SBH phases are present in their usual crystalline form in all examined samples. In the case of composites with CMCNa and PAANa, we can detect the presence of NaBr (marked with stars). The presence of another compound indicates that $SrBr_2$ has reacted with Na-ions during synthesis, which were used to neutralise the polymer, and it precipitated in the form NaBr. This further suggests that a partial ion exchange might have happened (Na^+ vs Sr^{2+}). Anionic polymers frequently capture divalent ions, leading to gelation and lower solubility. Those structures are hence stabilized while not participating in an equilibrium situation in solution. The polymer itself is most likely neutralised with Sr^{2+} as we did not detect other phases.

The presence of PDAC in the composite (blue curve) leads to peak broadening and a peak shift to higher 2θ, which we will evaluate in more detail in the following section. Because the initial screening measurements show a significant shift in hydration temperature and crystal structure only in the presence of PDAC, the remainder of the paper will focus on the SBH_G_PDAC composites. Most attention will be given to the hydration of SBM and how it is affected by varying PDAC content.

3.1.3. Impact of PDAC content on (de)hydration onset points

In this section, we once again explore the phase diagram. Similarly to pure SBH, (de)hydration onset points for composites with PDAC were determined for a wide range of vapour pressures (4, 8, 12, 15 mbar between 25 and 60 °C), and they are summarised in Fig. 7. This figure shows that the addition of small amounts of PDAC (0.1 g PDAC: 5 g SBH, green triangles) has a marginal effect on the location of the reaction onset points. We observe a significant lowering of the hydration onset points with an increased amount of PDAC (1 g PDAC: 5 g SBH, red triangles). When the measurement was conducted at 4 mbar p_{vap}, hydration was not observed for SBH_G_PDAC(1) sample within the measurement temperature window, which means that the hydration temperature is lower than 25 °C at this vapour pressure. The shift in dehydration temperature never exceeds 1 °C, and it is within the experimental error margin. Thus, we conclude that PDAC has a negligible impact on the onset of dehydration of SBH.

3.2. Impact of PDAC on the crystalline phases of $SrBr_2$

In the previous section, we have shown that PDAC affects the hydration of SBM and that it has almost no impact on the dehydration of SBH and that this effect is dependent on the polymer content in the composite. In this section, we zoom in on the effects of varying PDAC content on the crystal habit. For this purpose, we have extended our initial screening XRD measurements by two additional polymer contents while maintaining the same sample preparation and measurement method.

Initial analysis of XRD spectra in Fig. 8 shows a peak shift to higher 2θ with increasing PDAC content. This observation indicates increasing strain in the crystal lattice of the SBM and SBH phase, which can be estimated with the Halder-Wagner method [43] included in the PDXL2

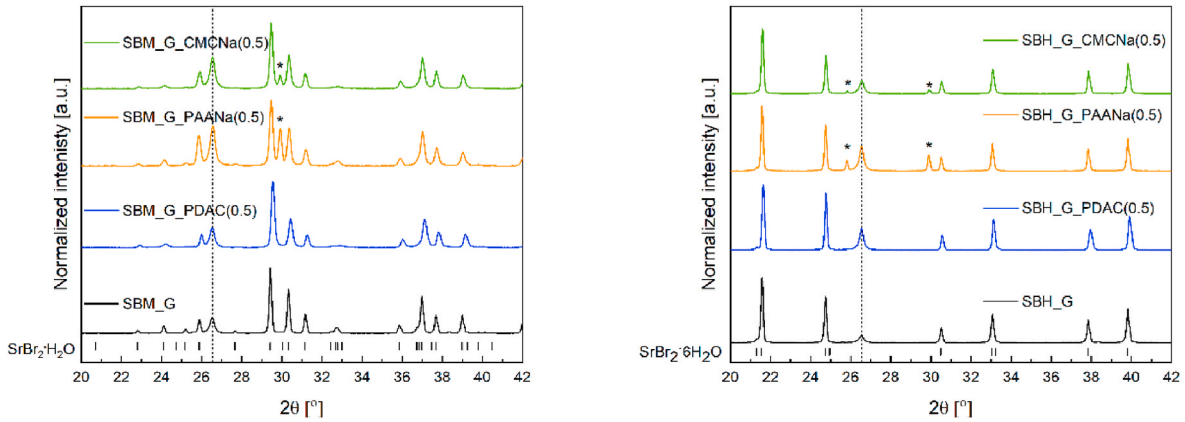

Fig. 6. XRD diffractograms of investigated composites with SrBr2 a) monohydrate (COD 1528458) and b) hexahydrate (COD 2003194). The dashed line indicates graphite 002 peak (COD 9011577), the star indicates NaBr peaks (COD 9007465).

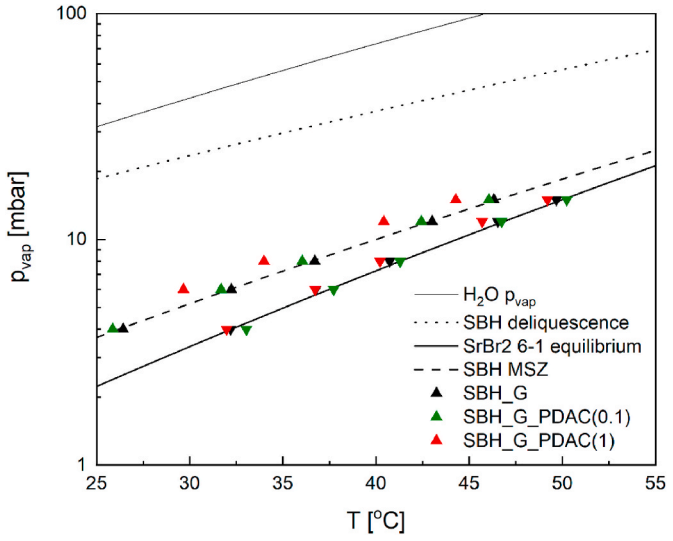

Fig. 7. p-T phase diagram of $SrBr_2$ with measured reaction onset for SBH_G (black), SBG_G_PDAC(0.1) (green), and SBG_G_PDAC(1) (red). Upwards pointing triangles show hydration onset point, downwards pointing triangles show dehydration onset point. (For interpretation of the references to colour in this figure legend, the reader is referred to the Web version of this article.)

software. The methodology describes peak broadening with symmetric Voight function and utilises the relationship between calculated full width half maximum and lattice distance at given lattice plane to calculate the average crystallite size and strain. A more detailed analysis revealed that SBM samples with large amounts of PDAC (0.5–1 g: 5 g SBH) have approximately 0.12–0.15 ± 0.09% strain. Comparatively, the only composite with SBH that exhibits lattice strain in the order of 0.09 ± 0.04% is SBH_G_PDAC(1).

Further analysis with the aid of the Scherrer formula, which determines the crystallite size based on a full-width half-maximum of a peak, shows that with the addition of PDAC, the size of primary scattering domains is reduced by approximately 44% with respect to SBH_G and by approximately 50% with respect to SBM_G, as shown in Fig. 9. The modification of crystallisation behaviour could cause this by PDAC, which has been observed in other studies [36]. In all cases, the impact on the crystallite size is more prominent for SBM than for SBH. Furthermore, a spread in the estimated crystallite size is seen with increased PDAC content, indicating that various lattice planes might be affected differently.

To test the theory of preferential binding, in Fig. 10 we compare peak areas of the most prominent peaks. In most cases, the peak area decreases with respect to the $SrBr_2$_G composite, which we use as reference material in this analysis. Therefore, we assume that only peaks with an area smaller than those of the mean peak area plus/minus the deviation can be considered severely impacted by the presence of PDAC. In the case of SBM composites, we observe the strongest impact for (2,0,1) and (3,0,1) planes. Unfortunately, we cannot draw any clear conclusion from that observation. For SBH composites, the most affected planes are

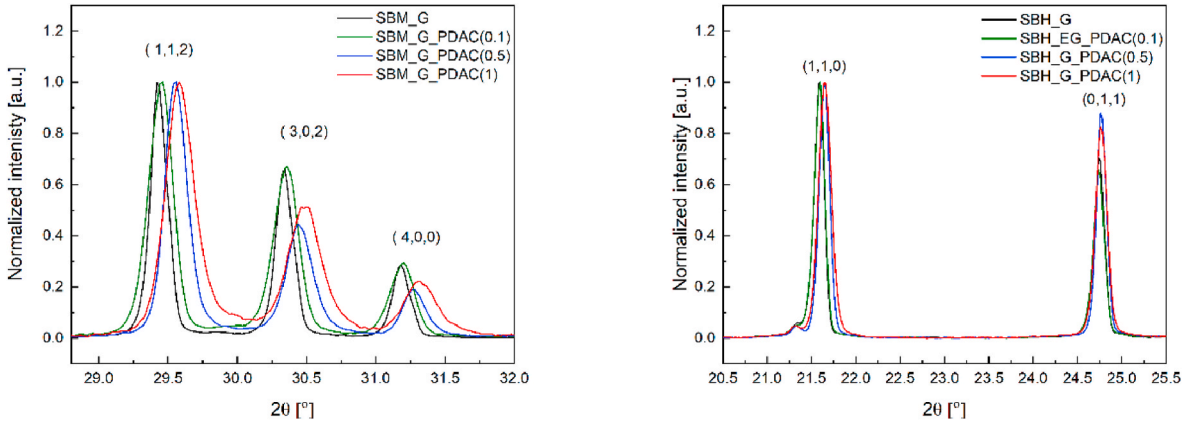

Fig. 8. Magnification of most characteristic peaks of a) SBM and b) SBH composites normalised w.r.t (1,1,2) plane for SBM and (1.1.0) plane for SBH composites. Corresponding lattice planes are indicated above the peaks.

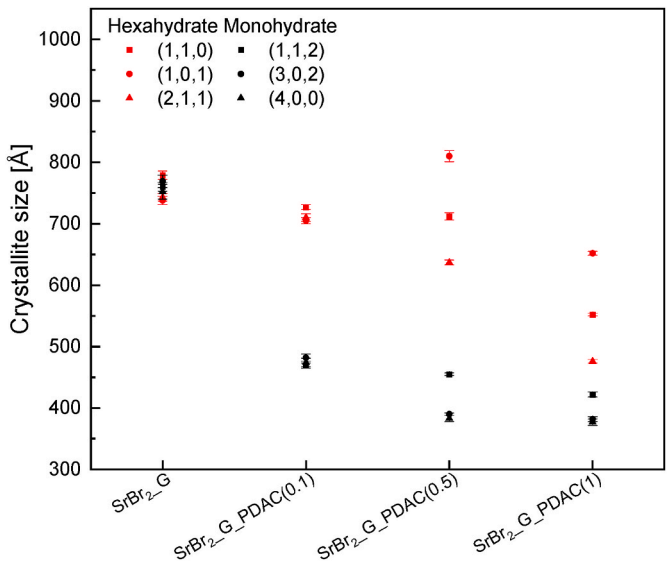

Fig. 9. Crystallite size calculated based on Scherrer formula for three most characteristic peaks of SBH (red) and SBM (black) composites with their respective error bars. (For interpretation of the references to colour in this figure legend, the reader is referred to the Web version of this article.)

(1,1,0) and (1,1,1). The particularly strong effect on (1.1.0) plane is interesting as this plane comprises in a large degree of Br-atoms, which can interact with the positively charged groups on PDAC. Nevertheless, a dedicated study is necessary to understand this crystallographic phenomenon fully.

3.3. Impact of PDAC on crystal growth

To better evaluate the impact of PDAC on the crystallisation of SBH, single crystals were grown through evaporation of solution for 90–100 days. An example of the representative crystals is shown in Fig. 11, with millimetre paper as a backdrop. Pure SBH crystallises as elongated, see-through needles with a few tens of micrometre in diameter. The addition of NMP to the base solution results in the growth of very fine needles thinner and shorter than the needles of pure SBH. It shows that ternary amines can impact the crystallisation behaviour of SBH even when they are not existent as polymers. The addition of PDAC to the base solution resulted in the growth of a large single crystal with a dendritic growth pattern showing on the bottom of the crystal, which is common in diffusion limited processes [44].

3.4. Water sorption properties of pure PDAC

To understand the effect PDAC has on the hydration of SBM and its contribution to the overall water absorption by the composite, the behaviour of pure PDAC in a relevant p-T window has to be understood. For this purpose, we have conducted DVS measurements (0–60% RH at 25, 35 and 40 °C) on dry PDAC powder. Fig. 12 shows that pure polymer exhibits minimal hysteresis between water sorption and desorption and that it can absorb significant amounts of water per mole monomer (DADMAC).

From this data, isosteric heat of sorption, q_{st}, can be obtained [45]. Fig. 13 shows that q_{st} varies with the overall water content in the polymer and is comparable with the values obtained for other highly hydrophilic polymers [46]. The corresponding Gibbs free energy varies from 14.25 kJ/mol H_2O for the first 0.5 mol H_2O/mol DADMAC to 2.99 kJ/mol H_2O for the third mol H_2O/mol DADMAC. For comparison,

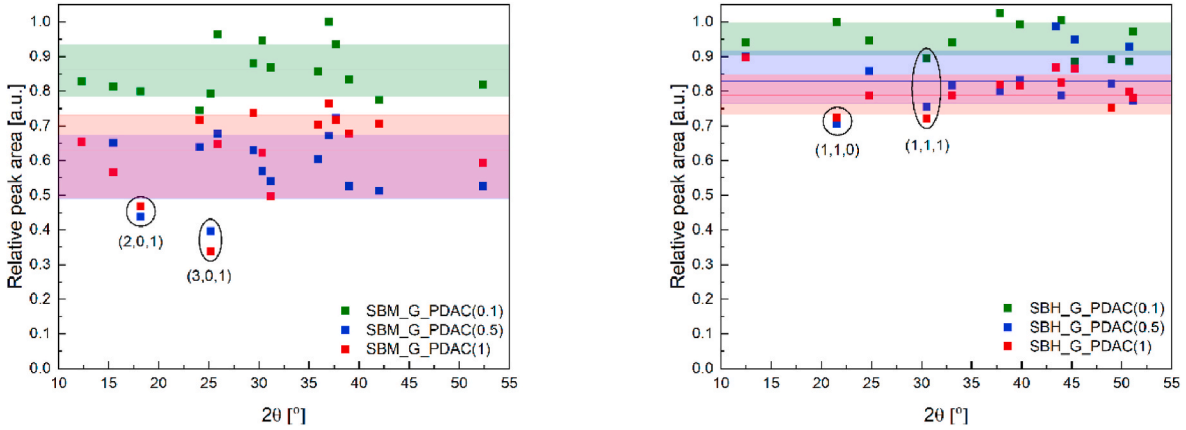

Fig. 10. Peak areas normalised w.r.t $SrBr_2$_G vs ideal 2θ positions of respective peaks for a) SBM composites and b) SBH composites. Horizontal lines indicate a given composite's mean relative peak area, and coloured areas are the standard deviations.

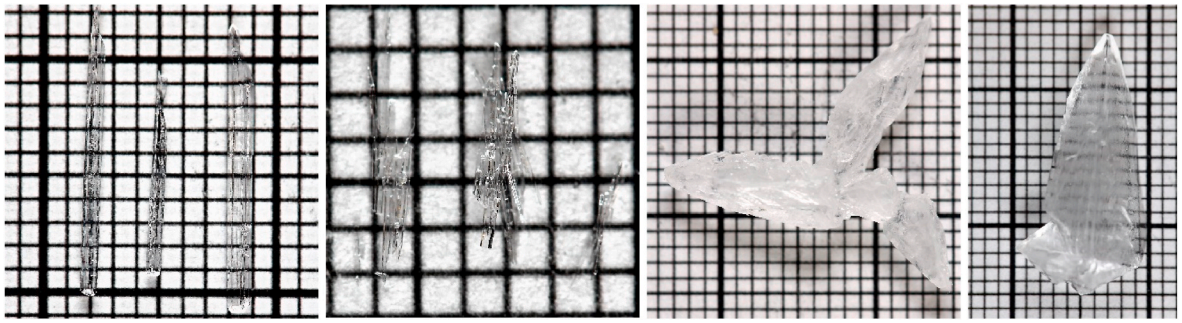

Fig. 11. SBH single crystals grown from solution a) SBH, b) SBH_NMP, c) SBH_PDAC(1) and d) SBH_PDAC(0.1). Millimetre paper is used as a backdrop.

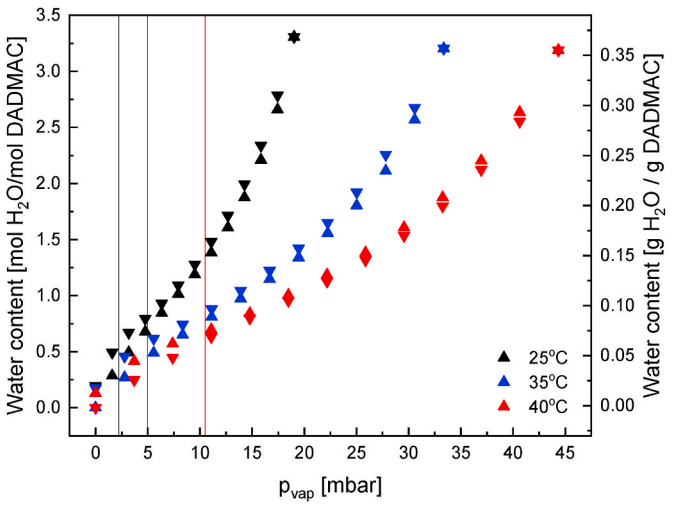

Fig. 12. Sorption (▲) and desorption (▼) isotherms of pure PDAC at 25 °C (black), 35 °C (blue) and 40 °C (red). Vertical lines indicate equilibrium vapour pressure for SBH-SBM reaction at respective temperatures. (For interpretation of the references to colour in this figure legend, the reader is referred to the Web version of this article.)

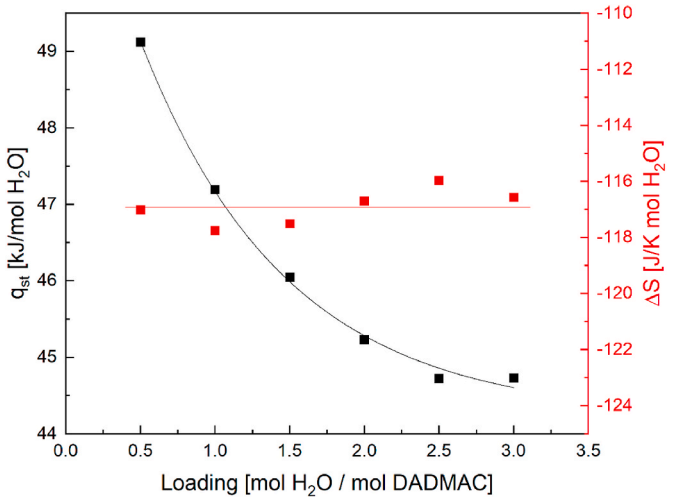

Fig. 13. Calculated steric heat of sorption, q_{st}, as a function of water content in PDAC powder (black) and the corresponding entropy (red). (For interpretation of the references to colour in this figure legend, the reader is referred to the Web version of this article.)

Glasser [47] has calculated the Gibbs free energy for hydration of SBM to be 15 kJ/mol H_2O and the reaction enthalpy to be 57.9 kJ/mol H_2O, showing that the energy involved in binding water to PDAC is comparable to the heat evolved during hydration of SBM. Moreover the enthalpy change for water absorption by PDAC is lower than hydration enthalpy of SBH. This means that less energy is lost during water binding to PDAC than to SBM, which in turn can promote the reaction with the polymer over salt.

3.5. Impact of PDAC on nucleation and growth

The lowering of the onset temperature for hydration induced by PDAC indicates inhibition of hydration reaction. Furthermore, the XRD study has shown that the crystal structure of both SBM and SBH is modified in the presence of PDAC, suggesting that the polymer impacts crystal growth, which is further supported by the single crystal growth study. This section will investigate the role PDAC plays in the overall hydration process through two sets of experiments. Firstly, we consider the impact of Cl^- counterion of PDAC on hydration reaction. Secondly, we explore the nucleation and growth processes occurring in the composite during hydration.

As PDAC is neutralised with Cl-ions, the typical Cl^-: Br^- ratio present in the samples varies between 0.02 and 0.16 (see Table 1). Further, the theoretical equilibrium line between $SrCl_2$ di- and monohydrate lies several degrees above the measured equilibrium of $SrBr_2$ hexa-monohydrate [47]. Therefore, it is conceivable that Cl^--Br^-- ion interaction could occur. To probe this possibility, we have synthesised and characterised a composite consisting of $SrCl_2{\cdot}6H_2O$, graphite and PDAC (3.75 g: 1 g: 1 g) identically to SBH-composites. Hydration behaviour for 1–2 transition of the SCH-composite and pure $SrCl_2$ (85-30 °C at 9, 12 and 15 mbar) is summarised in Fig. 14. It shows that in all cases, samples with PDAC (solid lines) exhibit lowering of hydration temperature compared to pure SCM (dashed lines), as indicated by the arrows. Since the only anion present in this composite is Cl^-, there is no possibility for ion exchange between salt and polymer. It means that the lower hydration temperature observed in SBH-PDAC composites is not due to Cl-Sr interaction, as we have observed the same interaction between SCH and PDAC.

To understand this interaction, we have conducted a more detailed nucleation and growth study in the SBH-PDAC system. This study was carried out at isothermal and isobaric conditions close to MSZ of pure SBH (see red dots in Fig. 3). Two samples, one with PDAC (SBH_G_PDAC (1)) and one without (SBH_G), were subjected to those measurements. Firstly, the investigated sample was dehydrated to monohydrate in-situ (80 °C, 0 mbar). Subsequently, the temperature was lowered to 30 °C and only after an equilibration period of 30min the water vapour (p_{vap} = 5 mbar) was introduced to the system (t=0 in Fig. 15). In the first test, vapour pressure was held fixed throughout the entire measurement (black curves). In this case, sample without PDAC begins to hydrate after approximately 45min of the induction period within MSZ. The sample with PDAC increases in mass rapidly after the water vapour is introduced. However, the mass levels off after 30 min showing a 2% mass increase with respect to the initial sample mass. This slight mass increase is partially due to water sorption by PDAC. Based on DVS measurements of pure PDAC, we expect a mass increase of approximately 1% at those conditions. However, the presence of salt in the composite might affect

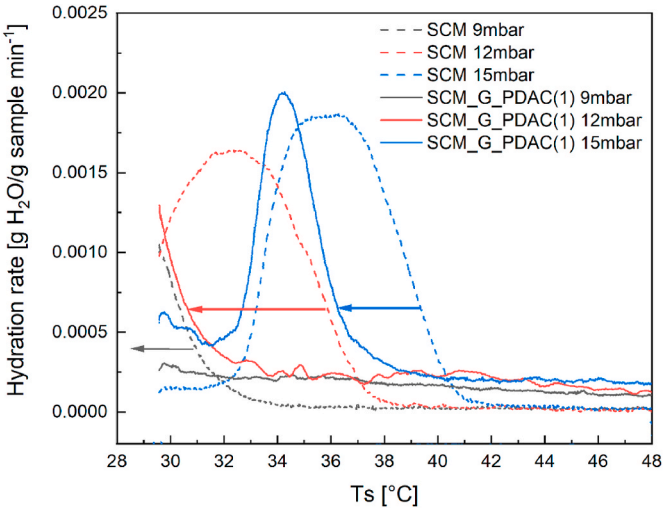

Fig. 14. First derivative of a mass curve plotted against measured sample temperature for pure $SrCl_2{\cdot}H_2O$ (SCM, dashed lines) and SCM_EG_PDAC(1) composite (solid lines) at a fixed vapour pressure of 9 mbar (black), 12 mbar (red) and 15 mbar (blue). Arrows indicate a shift in the measured onset of transition is between $SrCl_2$ 1–2 hydrate. (For interpretation of the references to colour in this figure legend, the reader is referred to the Web version of this article.)

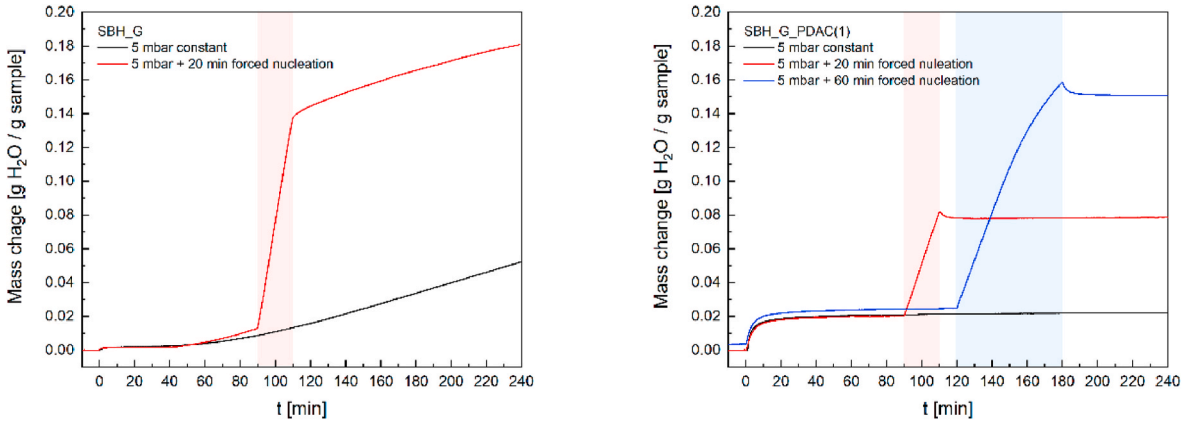

Fig. 15. Nucleation and growth studies at a fixed temperature of 30 °C and vapour pressure of 5 mbar conducted on a) SBH_G and b)SBH_G_PDAC(1). Black curves correspond to measurements without a forced nucleation period, while coloured curves correspond to measurements with a forced nucleation period at 8 mbar. This period is indicated by the coloured zones: red – 20min, blue 60min. (For interpretation of the references to colour in this figure legend, the reader is referred to the Web version of this article.)

the sorption properties of PDAC [48]. We, therefore, conclude that no hydration of SBM is observed within the allocated 4 h.

In the second test (red curves), the sample was conditioned the same way as in the first measurement. Additionally, after 1 h at 5 mbar, hydration reaction was aided with a 20min nucleation period outside of MSZ (8 mbar, marked in grey). A rapid mass increase is observed in both composites at those conditions as they are far from MSZ. When vapour pressure is reduced back to 5 mbar, the sample without PDAC continues to hydrate. The hydration rate after nucleation at 8 mbar is comparable with rates of not nucleated samples. On the contrary, mass uptake for the sample with PDAC halts completely.

A sample with PDAC was subjected to a third test (blue line) where it was nucleated for 60min. Once again, after the nucleation period at elevated vapour pressure, further hydration stops completely when conditions are returned to MSZ. In all cases, the mass uptake during the nucleation period outside of MSZ is greater than the water uptake of PDAC alone thus, a partial conversion from SBM to SBH must have occurred. Despite that, the hydration reaction does not continue for the sample with PDAC after returning to MSZ. Those results show that PDAC impacts the nucleation of SBH and its growth.

3.6. Impact of PDAC on (de)hydration kinetics

With the impact of PDAC on hydration within MSZ evaluated, we investigated the reaction kinetics of four composites at isobaric and isothermal conditions, specified in Section 2.3.2. Reaction kinetics are measured after the initial 10 (de)hydration cycles, to obtain a relatively stable kinetic. The kinetics measurements follow the same principle as the nucleation and growth study. Four measurements in two pairs are conducted at 45 °C. One of the sets is close to equilibrium conditions and the other further away. The pairs of conditions were defined such that $p_{eq}/p_{hyd} \approx p_{deh}/p_{eq}$. In classical nucleation theory, this relationship describes the driving force.

When hydration is evaluated far from the MSZ (21 mbar, Fig. 16a) and the driving force is large, the reaction speed is nearly doubled by adding low amounts of PDAC (0.1 g: 5g SBH). Composites with larger amounts of PDAC show an initial rapid water uptake by the polymer, but the salt hydration speed is hampered by 30–40% compared to SBH_G. In the case of hydration at the edge of MSZ, where the driving force is small (14 mbar, Fig. 16b), the impact of low amounts of PDAC is negligible. Higher amounts prevent hydration at those conditions, similar to what we observed earlier in nucleation and growth studies. The observed mass uptake is most likely due to water uptake by the polymer, although the calculated value is twice as high compared to the data obtained with pure PDAC. In all cases, the induction time is measured at the edge of the MSZ boundary, and the addition of PDAC prolongs this period.

When investigating the dehydration process far from equilibrium conditions, we see that low amounts of PDAC have a beneficial impact on the kinetics, which are nearly doubled, as shown in Fig. 17. However, PDAC retains some water at the end of the measurement, which can be

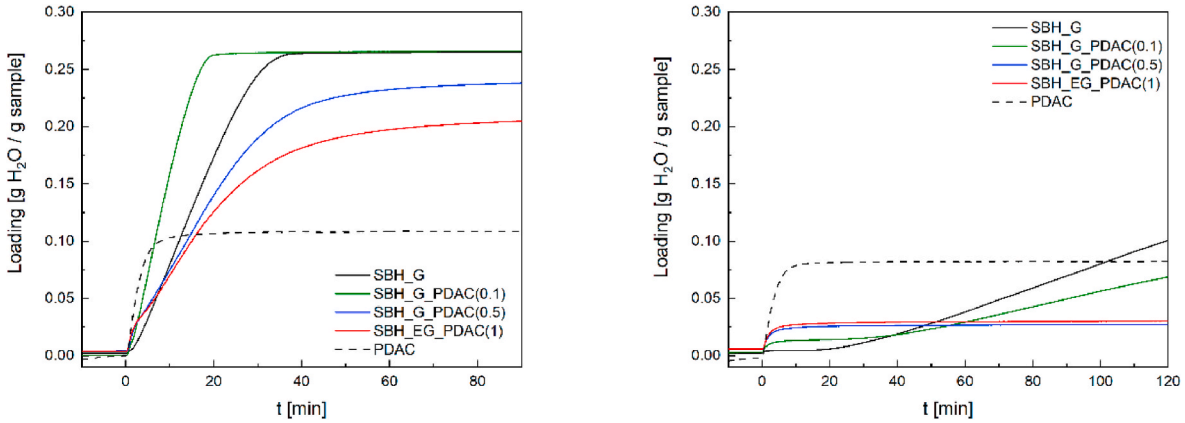

Fig. 16. Isobaric and isothermal hydration at 45 °C and a) 21 mbar and b) 9 mbar partial vapour pressure of SBH_G (black) and SBH_G_PDAC-polymers (coloured) The dashed plot shows water sorption of pure PDAC at identical conditions. (For interpretation of the references to colour in this figure legend, the reader is referred to the Web version of this article.)

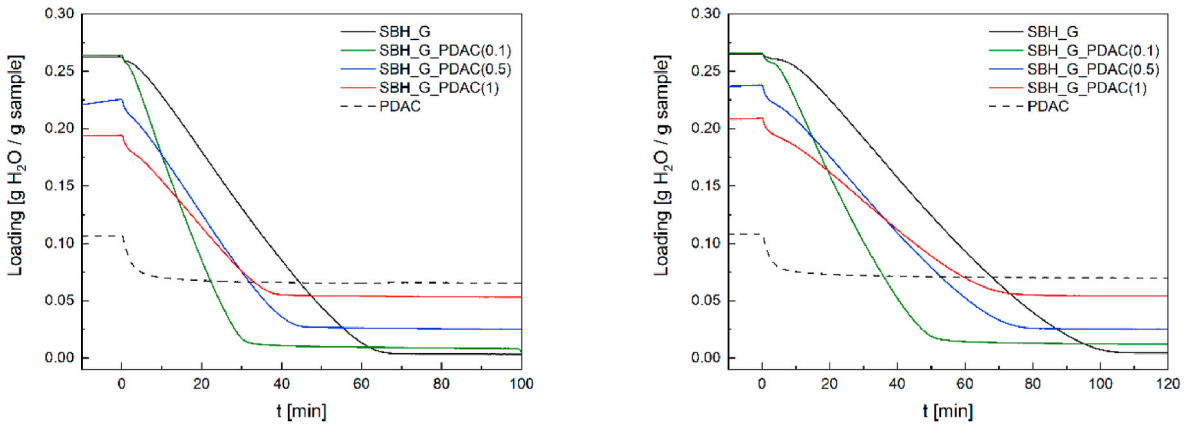

Fig. 17. Isobaric and isothermal dehydration at 45 °C and a) 8 mbar and b) 9 mbar partial vapour pressure of SBH_G (black) and SBH_G_PDAC-polymers (coloured). The dashed plot shows water sorption of pure PDAC at identical conditions. (For interpretation of the references to colour in this figure legend, the reader is referred to the Web version of this article.)

seen from the elevated end loading. This effect becomes more pronounced with larger amounts of polymer in the composite. Once again, the retained water content is higher than expected based on pure PDAC powder measurements. It should be noted that despite prolonged hydration, samples with large PDAC content did not achieve complete hydration within the allocated time (3 h), which might impact the measured dehydration speed. In the case of SBH_G_PDAC(0.5), this speed is comparable with composite without any polymer, while larger amounts of PDAC slow down the dehydration by 15–20%.

3.7. Kinetics during cycling

Finally, we look back at the hydration kinetics during the initial ten cycles which were conducted at 30 °C and 12 mbar. From the data summarised in Fig. 18, we see that all samples present stable hydration kinetics over at least 10 cycles. The first cycle for SBH_G deviates strongly from the remaining cycles (light grey plot), which is a known phenomenon amongst some salt hydrates [30,49]. On the contrary, samples with PDAC exhibit much more stable behaviour from the first cycle. In all cases a reproducible hydration is observed from at most 8th cycle confirming good material integrity previously observed by Salviati et al. [25].

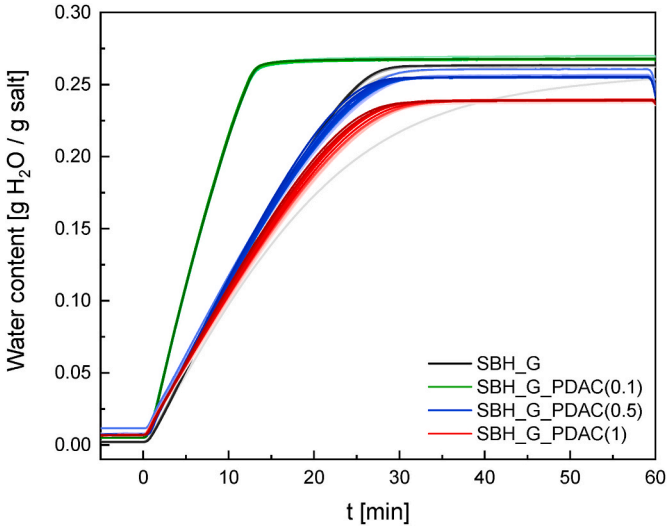

Fig. 18. Measured water content in the samples during pre-cycling. Hydration conducted at 30 °C and 12 mbar. The colour shades change from light to dark with increasing number of cycles. (For interpretation of the references to colour in this figure legend, the reader is referred to the Web version of this article.)

4. Discussion

As we have mentioned in the introduction, earlier works [31,33] suggest that phase transitions in salt hydrates with metastable behaviour advance through the formation of a wetting layer on the surface of the salt, dissolution of the lower hydrate in that wetting layer followed by crystallisation of a higher hydrate. The mobility of ions within the wetting layer is determinant for nucleation and growth, which can be related to the classical nucleation theory. Should the ionic mobility be affected, a change in hydration behaviour is expected.

We have shown that, similarly to K_2CO_3 or $CuCl_2$ in the study of Sögütoglu [31], $SrBr_2$ exhibits metastability during hydration of its monohydrate, see Fig. 4. It suggests that hydration of the monohydrate proceeds similarly and that a solution of $SrBr_2$ forms in the process. This solution is then in intimate contact with other composite components, which provides several modes of interaction. Both PAANa and CMCNa are weak anionic polymers [50] that were partially neutralised with sodium. However, neither of them has shown any interference during (de)hydration of SBM. This is most likely caused by the partial ion exchange of Na^+ with Sr^{2+} ions during preparation, as we discovered during XRD screening. On the other hand, PDAC is a cationic polymer with many amine groups and their Cl^- counterions that can interact with both Sr^{2+} and Br^- ions present in the wetting layer in many ways.

In Section 3.5, we have theorised that a potential conflict could arise from an interaction between Sr-ions and Cl-ions in the wetting layer. This could cause a shift in the equilibrium towards the formation of $SrCl_2$ instead of $SrBr_2$. Nevertheless, neither this nor the previous study [25] detected $SrCl_2$ hydrates in measured XRD patterns. Further, we have observed a similar shift in hydration for SCH composite, illustrated in Fig. 14. It proves that the widening of MSZ during hydration is not due to Cl-Br ion exchange between PDAC and $SrBr_2$, as this effect should not be present in a composite with only Cl-ions present in the wetting layer.

Nevertheless, the charged groups in PDAC can still interact with the ions in the wetting layer. This conflict could arise due to the potential complexation of Br-ions in the wetting layer. In solution, ternary and quaternary ammonium salts are known for their sequestration properties and ability to form complexes with a varying stoichiometry of counterions [51,52]. Such a mechanism could lower the mobility of Br-ions in the wetting layer and impact the nucleation and growth of SBH, which define the hydration process. A study investigating interactions between polydiallyldimethylammonium salt halides [53] has shown that they can bind iodine complexes from water solution.

Consequently, it could be expected that a similar process is possible for other halides as well. Our nucleation and growth study, presented in

Fig. 15, shows that large amounts of PDAC impact both processes. The inhibition of nucleation can be deduced from prolonged induction time within MSZ, where no hydration was observed for composite with PDAC. The growth inhibition is demonstrated by a lack of hydration after the intermediate nucleation period outside of MSZ. Br-complexation with Cl^- counterions through halogen bonds could cause both processes, thus suppressing hydration reaction at conditions within the MSZ, where SBM dissolution is limited.

Further evidence on how PDAC impacts SBH formation is found in the results of XRD measurements. From those, we can learn that PDAC influences the crystalline phases of both SBH and SBM. Those effects are primarily manifested through peak broadening and peak shift to higher 2θ with the addition of PDAC. The combination of both effects points towards increased strain in the crystal structure caused by out of equilibrium crystal growth [54]. The effect PDAC has on crystal growth is further demonstrated through its modification of crystal habit, which manifests itself through varying impact on the peak area of particularly (1,1,1) and (1,1,0) SBH crystal planes. Such out of equilibrium crystal growth is well demonstrated by the single crystals in Fig. 11. SBH is not the only compound whose morphology is affected by the presence of PDAC. Other studies [36,55] have shown that crystal morphology can vary due to the addition of PDAC. There it was postulated that polymer inhibits nucleation and growth of investigated salt. In addition, in an earlier SEM study by Salviati et al. [25] it has been shown that increasing PDAC content affects SBH distribution in the graphite matrix. It was postulated that the polyelectrolyte stabilized SBH crystals and prevents their aggregation in the matrix.

Finally, through isobaric and isothermal kinetics measurements, we have shown that small additions of PDAC (0.1 g: 5g SBH) can improve reaction hydration kinetics away from MSZ. This effect could be attributed to the hydrophilic properties of PDAC when in small quantities, it can facilitate water transport within the composite, but the concentration of amine groups is low enough not to interfere with the ionic mobility. More considerable additions create a barrier which, in the case of hydration reaction, will curb the kinetics far from MSZ and ultimately prevent the reaction from happening when close to MSZ. During dehydration, we have observed that the composites retain some water. Those amounts are larger than what is expected from the measurements conducted on pure polymer. We know that the polymer itself can retain a relatively large quantity of water, and the strength with which it is bound to the polymer can vary as well. This behaviour can be further modulated by ions present in the solution [48], which we assume is happening at those conditions.

5. Conclusions

In this study, we have investigated the impact of polymeric additives in SBH-G composites on the reaction kinetics of $SrBr_2$. Our investigation concerning the reaction onset points at 12 mbar vapour pressure have shown that from the investigated polymers (CMC, PAA and PDAC), only PDAC lowers the hydration temperature. The magnitude of the shift is dependent on PDAC content in the composite, and it increases with an increasing amount of polymer. Investigation of hydration kinetics has shown that small amounts of polymer can double the reaction speed, however excessive PDAC content can hamper hydration by 30–40% compared to SBH_G or even stop it completely.

Evaluation of dehydration behaviour has shown that neither of the investigated polymers has a significant impact on dehydration temperature, since the observed shifts are within measurement accuracy. The kinetic measurements show that similarly to hydration, dehydration speed is nearly doubled by adding small amounts of PDAC and decreases by 15–20% for larger PDAC contents. Additionally, part of the absorbed water is retained by PDAC at the end of dehydration.

Our XRD studies have shown that the crystalline nature of SBH and SBM are maintained in all composites. They also show a reduction of the primary domain size by 44–50% and an introduction of stress in the lattice with an increasing amount of PDAC. The mechanism underlying those observations is not fully understood at this moment and deserves a separate investigation.

Our TGA studies show that PDAC lowers hydration temperature due to a) inhibiting nucleation, which is inferred from measured induction times and b) hampering crystal growth at conditions where the driving force is low. The inhibition of nucleation and growth is ascribed to sequestering properties of ternary amines and the modification of crystal structure by the polymer. Nevertheless, when scant amounts of PDAC are present in a composite, the (de)hydration kinetics can be enhanced provided that the reaction takes place far from the MSZ. The enhanced kinetics are ascribed to the hydrophilic properties of the PDAC, which at low concentrations facilitates water transport in the composite.

CRediT authorship contribution statement

Natalia Mazur: Conceptualization, Methodology, Validation, Investigation, Visualization, Writing – original draft, Writing – review & editing. **Sergio Salviati:** Conceptualization, Resources, Writing – review & editing. **Henk Huinink:** Conceptualization, Writing – review & editing, Supervision, Funding acquisition. **Alberto Fina:** Conceptualization, Writing – review & editing. **Federico Carosio:** Conceptualization, Writing – review & editing. **Hartmut Fischer:** Conceptualization, Writing – review & editing, Supervision. **Olaf Adan:** Conceptualization, Writing – review & editing, Funding acquisition.

Declaration of competing interest

The authors declare that they have no known competing financial interests or personal relationships that could have appeared to influence the work reported in this paper.

Acknowledgements

This publication is part of the Mat4Heat project with project number 739.017.014 of the research programme Mat4Sus which is financed by the Dutch Research Council (NWO).

References

[1] S. Koohi-Fayegh, M.A. Rosen, A review of energy storage types, applications and recent developments, J. Energy Storage 27 (2020) 101047, https://doi.org/10.1016/j.est.2019.101047.
[2] I. Sarbu, A comprehensive review of thermal energy storage, Sustainability 10 (2018) 191, https://doi.org/10.3390/su10010191.
[3] L. Scapino, H.A. Zondag, J. Van Bael, J. Diriken, C.C.M. Rindt, Sorption heat storage for long-term low-temperature applications: a review on the advancements at material and prototype scale, Appl. Energy 190 (2017) 920–948, https://doi.org/10.1016/j.apenergy.2016.12.148.
[4] Y. Zhang, R. Wang, Sorption thermal energy storage: concept, process, applications and perspectives, Energy Storage Mater. 27 (2020) 352–369, https://doi.org/10.1016/j.ensm.2020.02.024.
[5] R.J. Clark, A. Mehrabadi, M. Farid, State of the art on salt hydrate thermochemical energy storage systems for use in building applications, J. Energy Storage 27 (2020) 101145, https://doi.org/10.1016/j.est.2019.101145.
[6] J. Lizana, R. Chacartegui, A. Barrios-Padura, C. Ortiz, Advanced low-carbon energy measures based on thermal energy storage in buildings: a review, Renew. Sustain. Energy Rev. 82 (2018) 3705–3749, https://doi.org/10.1016/j.rser.2017.10.093.
[7] D.M.R. Prasad, R. Senthilkumar, G. Lakshmanarao, S. Krishnan, B.S. Naveen Prasad, A critical review on thermal energy storage materials and systems for solar applications, AIMS Energy 7 (2019) 507–526, https://doi.org/10.3934/energy.2019.4.507.
[8] G.A. Farulla, M. Cellura, F. Guarino, M. Ferraro, A review of thermochemical energy storage systems for power grid support, Appl. Sci. 10 (2020), https://doi.org/10.3390/app10093142.
[9] H. Jarimi, D. Aydin, Z. Yanan, G. Ozankaya, X. Chen, S. Riffat, Review on the recent progress of thermochemical materials and processes for solar thermal energy storage and industrial waste heat recovery, Int. J. Low Carbon Technol. (2018) 1–26, https://doi.org/10.1093/ijlct/cty052.
[10] S.N. Gunasekara, C. Barreneche, A. Inés Fernández, A. Calderón, R. Ravotti, A. Ristić, et al., Thermal energy storage materials (TESMs)—what does it take to make them fly? Crystals 11 (2021) 1276, https://doi.org/10.3390/CRYST11111276, 2021;11:1276.

[11] S. Vasta, V. Brancato, D La Rosa, V. Palomba, G. Restuccia, A. Sapienza, et al., Adsorption heat storage: state of the art and future perspectives. https://doi.org/10.20944/PREPRINTS201806.0385.V1, 2018.

[12] P.A.J. Donkers, L. Pel, O.C.G. Adan, Experimental studies for the cyclability of salt hydrates for thermochemical heat storage, J. Energy Storage 5 (2016) 25–32, https://doi.org/10.1016/j.est.2015.11.005.

[13] H.U. Rammelberg, T. Osterland, B. Priehs, O. Opel, W.K.L. Ruck, Thermochemical heat storage materials – performance of mixed salt hydrates, Sol. Energy 136 (2016) 571–589, https://doi.org/10.1016/j.solener.2016.07.016.

[14] A. Solé, L. Miró, C. Barreneche, I. Martorell, L.F. Cabeza, Corrosion of metals and salt hydrates used for thermochemical energy storage, Renew. Energy 75 (2015) 519–523, https://doi.org/10.1016/j.renene.2014.09.059.

[15] F. Kleiner, K. Posern, A. Osburg, Thermal conductivity of selected salt hydrates for thermochemical solar heat storage applications measured by the light flash method, Appl. Therm. Eng. 113 (2017) 1189–1193, https://doi.org/10.1016/j.applthermaleng.2016.11.125.

[16] P.A.J. Donkers, L.C. Sögütoglu, H.P. Huinink, H.R. Fischer, O.C.G. Adan, A review of salt hydrates for seasonal heat storage in domestic applications, Appl. Energy 199 (2017) 45–68, https://doi.org/10.1016/j.apenergy.2017.04.080.

[17] M. Richter, E.M. Habermann, E. Siebecke, M. Linder, A systematic screening of salt hydrates as materials for a thermochemical heat transformer, Thermochim. Acta 659 (2018) 136–150, https://doi.org/10.1016/j.tca.2017.06.011.

[18] A. Fopah-Lele, J.G. Tamba, A review on the use of SrBr2·6H2O as a potential material for low temperature energy storage systems and building applications, Sol. Energy Mater. Sol. Cells 164 (2017) 175–187, https://doi.org/10.1016/j.solmat.2017.02.018.

[19] A. Fopah-Lele, C. Rohde, K. Neumann, T. Tietjen, A. Onnebeck, Kokouvi Edem N'tsoukpoe Tr€, T. Osterland, et al., Lab-scale experiment of a closed thermochemical heat storage system including honeycomb heat exchanger. https://doi.org/10.1016/j.energy.2016.08.009, 2016.

[20] B. Michel, N. Mazet, P. Neveu, Experimental investigation of an innovative thermochemical process operating with a hydrate salt and moist air for thermal storage of solar energy: global performance, Appl. Energy 129 (2014) 177–186, https://doi.org/10.1016/j.apenergy.2014.04.073.

[21] W. Li, H. Guo, M. Zeng, Q. Wang, Performance of SrBr2·6H2O based seasonal thermochemical heat storage in a novel multilayered sieve reactor, Energy Convers. Manag. 198 (2019) 111843, https://doi.org/10.1016/j.enconman.2019.111843.

[22] L.G. Gordeeva, Y.I. Aristov, Composites "salt inside porous matrix" for adsorption heat transformation: a current state-of-the-art and new trends, Int. J. Low Carbon Technol. 7 (2012) 288–302, https://doi.org/10.1093/ijlct/cts050.

[23] Y.J. Zhao, R.Z. Wang, Y.N. Zhang, N. Yu, Development of SrBr2 composite sorbents for a sorption thermal energy storage system to store low-temperature heat, Energy 115 (2016) 129–139, https://doi.org/10.1016/j.energy.2016.09.013.

[24] A. Cammarata, V. Verda, A. Sciacovelli, Y. Ding, Hybrid strontium bromide-natural graphite composites for low to medium temperature thermochemical energy storage: formulation, fabrication and performance investigation, Energy Convers. Manag. 166 (2018) 233–240, https://doi.org/10.1016/j.enconman.2018.04.031.

[25] S. Salviati, F. Carosio, G. Saracco, A. Fina, Hydrated salt/graphite/polyelectrolyte organic-inorganic hybrids for efficient thermochemical storage, Nanomaterials 9 (2019) 15121, https://doi.org/10.3390/nano9030420.

[26] S. Salviati, F. Carosio, F. Cantamessa, L. Medina, L.A. Berglund, G. Saracco, et al., Ice-templated nanocellulose porous structure enhances thermochemical storage kinetics in hydrated salt/graphite composites, Renew. Energy 160 (2020) 698–706, https://doi.org/10.1016/j.renene.2020.07.036.

[27] P. D'Ans, E. Courbon, A. Permyakova, F. Nouar, C. Simonnet-Jégat, F. Bourdreux, et al., A new strontium bromide MOF composite with improved performance for solar energy storage application, J. Energy Storage 25 (2019) 100881, https://doi.org/10.1016/J.EST.2019.100881.

[28] E. Courbon, P. D'Ans, A. Permyakova, O. Skrylnyk, N. Steunou, M. Degrez, et al., A new composite sorbent based on SrBr2 and silica gel for solar energy storage application with high energy storage density and stability, Appl. Energy 190 (2017) 1184–1194, https://doi.org/10.1016/J.APENERGY.2017.01.041.

[29] B. Ding, C. Xu, Z. Liao, F. Ye, Study on long-term thermochemical thermal storage performance based on SrBr2-expanded vermiculite composite materials, J. Energy Storage 42 (2021) 103081, https://doi.org/10.1016/J.EST.2021.103081.

[30] L.C. Sögütoglu, P.A.J. Donkers, H.R. Fischer, H.P. Huinink, O.C.G. Adan, In-depth investigation of thermochemical performance in a heat battery: cyclic analysis of K2CO3, MgCl2and Na2S, Appl. Energy 215 (2018) 159–173, https://doi.org/10.1016/j.apenergy.2018.01.083.

[31] L.C. Sögütoglu, M. Steiger, J. Houben, D. Biemans, H.R. Fischer, P. Donkers, et al., Understanding the hydration process of salts: the impact of a nucleation barrier, Cryst. Growth Des. 19 (2019) 2279–2288, https://doi.org/10.1021/acs.cgd.8b01908.

[32] L.C. Sögütoglu, F. Birkelbach, A. Werner, H. Fischer, H. Huinink, O. Adan, Hydration of salts as a two-step process: water adsorption and hydrate formation, Thermochim. Acta 695 (2021), https://doi.org/10.1016/j.tca.2020.178819.

[33] K. Linnow, M. Niermann, D. Bonatz, K. Posern, M. Steiger, Experimental studies of the mechanism and kinetics of hydration reactions, Energy Proc. 48 (2014) 394–404, https://doi.org/10.1016/j.egypro.2014.02.046.

[34] K.N. Olafson, R. Li, B.G. Alamani, J.D. Rimer, Engineering crystal modifiers: bridging classical and nonclassical crystallization, Chem. Mater. 28 (2016) 8453–8465, https://doi.org/10.1021/acs.chemmater.6b03550.

[35] S. Radhakrishnan, D.R. Saini, Polymer-induced crystallization of inorganic salts II. PEO-CaCl2, PEO-K2CO3 and PEO-CaCO3, J. Cryst. Growth 129 (1993) 191–201, https://doi.org/10.1016/0022-0248(93)90448-6.

[36] J. Kim, S.H. Yang, formation of pyramidal calcite and amorphous calcium carbonate films by cationic polyelectrolytes, poly(diallyldimethylammonium chloride), Bull. Kor. Chem. Soc. 38 (2017) 1238–1241, https://doi.org/10.1002/bkcs.11237.

[37] Z. Amjad, Inhibition of calcium fluoride crystal growth by polyelectrolytes, Langmuir 7 (1991) 2405–2408, https://doi.org/10.1021/la00058a072.

[38] W. Dungkaew, K.J. Haller, A.E. Flood, J.F. Scamehorn, Crystallization of low solubility calcium-arsenate compounds for arsenic removal from poly (diallyldimethyl ammonium chloride)- arsenate solution, AIChE Annu. Meet. Conf. Proc. 4 (2006) 64–75.

[39] L. Greenspan, Humidity fixed points of binary saturated aqueous solutions, J Res Natl Bur Stand - A Phys Ics Chem 82A (1976) 89–96.

[40] M.A. Stanish, D.D. Perlmutter, Rate processes in cycling a reversible gas-solid reaction, AIChE J. 30 (1984) 56–62, https://doi.org/10.1002/aic.690300110.

[41] A. Vaitkus, A. Merkys, S. Gražulis, Validation of the Crystallography open database using the crystallographic information framework, J. Appl. Crystallogr. 54 (2021) 661–672, https://doi.org/10.1107/s1600576720016532.

[42] P.J. Halling, Salt hydrates for water activity control with biocatalysts in organic media, Biotechnol. Tech. 6 (1992) 271–276, https://doi.org/10.1007/BF02439357.

[43] D. Nath, F. Singh, R. Das, X-ray diffraction analysis by Williamson-Hall, Halder-Wagner and size-strain plot methods of CdSe nanoparticles- a comparative study, Mater. Chem. Phys. 239 (2020) 122021, https://doi.org/10.1016/j.matchemphys.2019.122021.

[44] M.E. Glicksman, A.O. Lupulescu, Dendritic crystal growth in pure materials, J. Cryst. Growth 264 (2004) 541–549, https://doi.org/10.1016/j.jcrysgro.2003.12.034. North-Holland.

[45] M.D. Torres, R. Moreira, F. Chenlo, M.J. Vázquez, Water adsorption isotherms of carboxymethyl cellulose, guar, locust bean, tragacanth and xanthan gums, Carbohydr. Polym. 89 (2012) 592–598, https://doi.org/10.1016/j.carbpol.2012.03.055.

[46] H. Kusanagi, S. Yukawa, Fourier transform infra-red spectroscopic studies of water molecules sorbed in solid polymers, Polymer 35 (1994) 5637–5640, https://doi.org/10.1016/S0032-3861(05)80037-0.

[47] L. Glasser, Thermodynamics of inorganic hydration and of humidity control, with an extensive database of salt hydrate pairs, J. Chem. Eng. Data 59 (2014) 526–530, https://doi.org/10.1021/je401077x.

[48] R. Zhang, Y. Zhang, H.S. Antila, J.L. Lutkenhaus, M. Sammalkorpi, Role of salt and water in the plasticization of PDAC/PSS polyelectrolyte assemblies, J. Phys. Chem. B 121 (2017) 322–333, https://doi.org/10.1021/acs.jpcb.6b12315.

[49] M.A. Stanish, D.D. Perlmutter, Kinetics of hydration-dehydration reactions considered as solid transformations, AIChE J. 30 (1984) 557–563, https://doi.org/10.1002/aic.690300405.

[50] J. Fu, H.M. Fares, J.B. Schlenoff, Ion-pairing strength in polyelectrolyte complexes, Macromolecules 50 (2017) 1066–1074, https://doi.org/10.1021/acs.macromol.6b02445.

[51] Y.A. Hugo, N. Mazur, W. Kout, F. Sikkema, Z. Borneman, K. Nijmeijer, Effect of bromine complexing agents on membrane performance in hydrogen bromine flow batteries, J. Electrochem. Soc. 166 (2019) A3004–A3010, https://doi.org/10.1149/2.0951913jes.

[52] S.N. Bajpai, Vapor pressures of bromine-quaternary ammonium salt complexes for zinc-bromine battery applications, J. Chem. Eng. Data 26 (1981) 2–4, https://doi.org/10.1021/je00023a002.

[53] J. Bendoraitiene, E. Mazoniene, R.J. Zemaitaitiene, A. Zemaitaitis, Interaction of polydiallyldimethylammonium salts with iodine, J. Appl. Polym. Sci. 100 (2006) 2710–2716, https://doi.org/10.1002/app.23004.

[54] S.J.C. Granneman, B. Lubelli, van Hees Rpj, Mitigating salt damage in building materials by the use of crystallization modifiers – a review and outlook, J. Cult. Herit. 40 (2019) 183–194, https://doi.org/10.1016/j.culher.2019.05.004.

[55] S.P. Garcia, S. Semancik, Controlling the morphology of zinc oxide nanorods crystallized from aqueous solutions: the effect of crystal growth modifiers on aspect ratio, Chem. Mater. 19 (2007) 4016–4022, https://doi.org/10.1021/cm061977r.